EARTHQUAKE SPECTRA

The Professional Journal of the Earthquake Engineering Research Institute

PREPRINT

This preprint is a PDF of a manuscript that has been accepted for publication in *Earthquake Spectra*. It is the final version that was uploaded and approved by the author(s). While the paper has been through the usual rigorous peer review process for the Journal, it has not been copyedited, nor have the figures and tables been modified for final publication. Please also note that the paper may refer to online Appendices that are not yet available.

We have posted this preliminary version of the manuscript online in the interest of making the scientific findings available for distribution and citation as quickly as possible following acceptance. However, readers should be aware that the final, published version will look different from this version and may also have some differences in content.

The DOI for this manuscript and the correct format for citing the paper are given at the top of the online (html) abstract.

Once the final, published version of this paper is posted online, it will replace the preliminary version at the specified DOI.

Tests on Thin Reinforced Concrete Walls Subjected to In-plane and Out-of-plane Cyclic Loading

João Almeida,[a)] Ovidiu Prodan,[a)] Angelica Rosso,[a)] and Katrin Beyer,[a)] M.EERI

The present data paper describes an experimental campaign on five thin T-shaped reinforced concrete walls, including: details on the test units, materials, test setup, loading protocol, instrumentation, main features of each unit's response, organization of the provided test data, and examples of derived data. The tests aimed at assessing the influence of wall thickness on member stability, the role of lap splices on damage distribution and displacement ductility, and the effects of the simultaneous application of out-of-plane loading on the member response. A set of five companion test reports, one for each of the tested units, supplement the present manuscript.

INTRODUCTION

Recent earthquakes in Chile (2010) and New Zealand (2011) damaged a significant number of buildings with reinforced concrete (RC) walls. Failure modes that were observed after these events included out-of-plane failure of thin walls and failure of walls with lap splices (Kam, Pampanin, and Elwood 2011; Wallace et al. 2012; Elwood 2013; Sritharan et al. 2014). To investigate these failure modes and to analyse the effect of bi-directional loading on wall behaviour, an experimental program consisting of five specimens, tested at a scale that varied between 2/3 and 1/1 (full scale), was carried out at the *Earthquake Engineering and Structural Dynamics Laboratory (EESD Lab)*, *École Polytechnique Fédérale de Lausanne (EPFL)*,

[a)] Earthquake Engineering and Structural Dynamics Laboratory (EESD), School of Architecture, Civil and Environmental Engineering (ENAC), École Polytechnique Fédérale de Lausanne (EPFL), 1015 Lausanne, Switzerland

Switzerland, with the objective to complement existing data with regard to the aforementioned failure modes.

The walls had all the same cross-section (rectangular section with a small flange at one end) but different wall thicknesses and reinforcement layouts. The tests were quasi-static cyclic tests. Only the ground storey of the idealized walls was constructed and the axial force, shear forces and bending moments resulting from the upper storeys were simulated by three (in the uni-directional tests) or five (in the bi-directional tests) servo-controlled actuators. The first three walls (TW1 to TW3) were tested under in-plane loads, while the last two test units (TW4 and TW5) were subjected to a combination of in-plane and out-of-plane loads.

Wall TW1, which was geometrically identical to wall TW4, was tested in collaboration with the *School of Engineering of Antioquia* and the *University of Medellin*, Colombia. Reproducing a common current Colombian design trend for mid and high rise low-cost residential buildings, walls TW1 and TW4 have only a single layer of reinforcement. Additionally, since those walls have the smallest wall thickness and the largest shear span ratio, they are more prone to instability phenomena. A literature review (Rosso, Almeida, and Beyer 2015) on existing wall tests showing global out-of-plane instability of the member revealed that only seven tests from four different campaigns can be found (Oesterle et al. 1976; Goodsir 1985; Thomsen and Wallace 1995; Johnson 2010). All of these seven walls were subjected to uni-directional loading and their out-of-plane displacements along the wall height were either observed visually or measured at up to three different heights. The walls TW1 and TW4 of the present test campaign are unique as they provide, for the first time, data on the entire 3D displacement field of walls that develop large out-of-plane displacements. It is expected that these three-dimensional displacement fields of wall faces yield new insights into the development of the out-of-plane deformations, in particular with regard to: evolution of out-of-plane displacements along the height with imposed top in-plane displacements, portion of wall height and length that is involved in the out-of-plane instability, influence of both local and global tensile strains on the buckling behaviour, and role of bi-directional loading on out-of-plane instability (Rosso, Almeida, and Beyer 2016).

The geometrical and mechanical properties, as well as reinforcement detailing of test units TW2, TW3 and TW5 is meant to represent Swiss construction practice during the 50s-70s. It was characterized by wall thicknesses between 15 and 20 cm, longitudinal/transversal reinforcement ratios roughly between 0.3 and 0.8%, and transversal stirrups placed on the

inside of longitudinal rebars. It is noted that this latter uncommon constructional detail provides an unclear level of confinement to the concrete (which is dependent on the connection between the longitudinal and transversal reinforcement) and restraint against bar buckling. Wall lengths were typically very large, between 4 m and 9 m, while the concrete cover was quite thin, as low as 10 mm. In terms of lap splices, construction practice was to execute lap splices with a considerably low overlapping length of roughly around 30-35 times the diameter of the longitudinal rebar (the current code prescribes an overlapping length of 60 times the diameter). Walls TW2 and TW3 were tested to assess the influence of lap splices in the plastic hinge region. The effect of lap splices in the plastic zone at the wall base has been investigated by six research groups (Paterson and Mitchell 2003; Elnady 2008; Bimschas 2010; Birely 2012; Layssi and Mitchell 2012; Hannewald, Bimschas, and Dazio 2013; Villalobos 2014). Sixteen tests on walls with lap splices could be found in the literature, nine of which can be compared with a reference test without lap splices that has been conducted as well. The newly added pair (TW2, TW3) is unique with regard to its large ratio between lap splice length and shear span, which allows to investigate the effect of the moment gradient on the lap splice performance.

Finally, the effect of bi-directional loading on non-rectangular walls has been investigated in a number of experimental studies (e.g. Reynouard and Fardis 1993; Beyer, Dazio, and Priestley 2008; Brueggen 2009; Constantin and Beyer 2015). For rectangular or T-shaped walls such data is, however, not available. In order to address this research gap, walls TW4 and TW5—geometrically identical to walls TW1 and TW2 respectively—have been tested under bi-directional loading.

ORGANIZATION OF THE PAPER

This paper starts by presenting the geometry and the mechanical characterization of the test units, which is followed by the description of the test setup, the applied quasi-static cyclic loading protocol (both for uni- and bi-directional tests), and the instrumentation used. A summary of each of the test units' response is then presented, as well as the results for the in-plane global force-displacement response. A specific section is dedicated to explain the organization of the data (raw, processed and derived) for the five tests, which are shared online (Almeida, Prodan, Rosso, et al. 2016). Finally, a few examples of plots obtained from derived experimental data are given to illustrate how the data can be used to study local and global wall response parameters.

DESCRIPTION OF TEST UNITS AND MATERIALS

GEOMETRICAL CHARACTERIZATION

The test units were five T-shaped thin walls (the acronym 'TW' stands for 'thin wall') with a small flange, included to study the effect of a perpendicular wall on member stability and damage distribution. A summary of the main geometrical features, applied loading, and reinforcement details are listed in Table 1. The test units were designed in order to best represent the construction practices described in the Introduction.

Walls TW1 and TW4—whose cross-section is depicted in Figure 1(a)—were 2000 mm tall, 80 mm thick and 2700 mm long, with a lateral flange 80 mm thick and 440 mm long (see Figure 1(a)). The longitudinal reinforcement layout consisted of a single layer with 11 bars of diameter $d_w = 6$ mm (resulting in a geometric reinforcement ratio of $\rho_w = 0.15\%$ in the web), three additional bars of diameter $d_b = 16$ mm at the extremities (corresponding to a geometric reinforcement ratio of $\rho_b = 2.63\%$ in the boundary elements), and four bars of diameter $d_w = 6$ mm along the flange. The D6 longitudinal bars of TW1 and TW4 had 350 mm ($\sim 58 d_w$) long straight lap-splices at the bottom of the wall; the D16 bars were continuous. The transverse reinforcement ratio consisted of $d_t = 6$ mm bars at a spacing of $s_t = 200$ mm, yielding a geometric reinforcement ratio of $\rho_t = 0.18\%$. The shear span of these walls was fixed at 10 m, which corresponds to a shear span ratio of 3.70.

Walls TW2, TW3 and TW5—whose cross-section is depicted in Figure 1(b)—were 2000 mm tall, 120 mm thick and 2700 mm long, with a lateral flange 120 mm thick and 440 mm long (see Figure 1b)). The longitudinal reinforcement layout consisted of a double layer with a total of 58 bars of diameter $d_w = 6$ mm (resulting in a total longitudinal geometric reinforcement ratio of $\rho = 0.57\%$). Test unit TW3 had 216 mm ($36 d_w$) straight lap-splices at the bottom of the wall. The transverse reinforcement ratio consisted of $d_t = 6$ mm bars at a spacing of $s_t = 130$ mm (resulting in a geometric reinforcement ratio of $\rho_t = 0.36\%$). In the boundary elements 15 U-shaped rebars of diameter $d_h = 6$ mm at a spacing of $s_h = 130$ mm were placed. The concrete cover was 15 mm. The shear span of TW2 and TW3 was fixed at 3.15 m, which corresponds to a shear span ratio of 1.17. For TW5 the shear span was set to 7.35 m with the objective of rendering it more susceptible to out-of-plane instability.

The foundation of all the test units was 3600 mm long, 700 mm wide and 400 mm high, and it was designed as a stiff bearing for the walls. The foundation was fixed to the strong floor with six prestressed bars.

MECHANICAL CHARACTERIZATION

Concrete compression tests and double punch tests were carried out on cylinder specimens to determine the modulus of elasticity, compression strength, and tensile concrete strength for every wall. The results, corresponding to test averages, are summarized in Table 2.

The 6 mm diameter reinforcing steel rebars employed in all test units came from the same production batch, while the 16 mm rebars used in TW1 and TW4 came from different production batches. In order to describe their mechanical behaviour, the rebars were subjected to uniaxial tension tests. The corresponding results are summarized in Table 3.

Table 1. General geometrical features, applied loading, and reinforcement content of test units.

Test unit	TW1	TW2	TW3	TW4	TW5
Clear unsupported height	2 m	2 m	2 m	2 m	2 m
Length	2.7 m	2.7 m	2.7 m	2.7 m	2.7 m
Thickness	80 mm	120 mm	120 mm	80 mm	120 mm
Shear span	10 m	3.15 m	3.15 m	10 m	7.35 m
Applied shear span ratio	3.70	1.17	1.17	3.70	2.72
Axial load ratio[a]	0.043	0.032	0.034	0.033	0.048
Longitudinal reinforcement	15 × D6 + 6 × D16	66 × D6	66 × D6	15 × D6 + 6 × D16	66 × D6
Total longitudinal reinforcement ratio	0.67%	0.57%	0.57%	0.67%	0.57%
Web longitudinal reinforcement ratio	0.15%	0.50%	0.50%	0.15%	0.50%
Boundary element longitudinal reinforcement ratio[b]	2.63%	0.50%	0.50%	2.63%	0.50%
Lap splice length	350 mm[c]	-	216 mm[d]	350 mm[c]	-
Transverse reinforcement	D6 @ 200 mm	D6 @ 130 mm	D6 @ 130 mm	D6 @ 200 mm	D6 @ 130 mm
Transverse reinforcement ratio	0.18%	0.36%	0.36%	0.18%	0.36%

[a]Computed with concrete strength $f_{c,cyl}$ from Table 2. [b]The boundary element is defined as the 300 mm long region from the web edge where the larger diameter bars are placed. [c]Only the D6 bars were spliced; the D16 bars were continuous. [d]All the longitudinal bars were spliced.

Table 2. Results of concrete compression tests and double-punch tests.

Test unit	TW1	TW2	TW3	TW4	TW5
$f_{c,cyl}$ *(MPa)*	28.8	50.7	48.3	31.2	33.6
f_t *(MPa)*	2.2	2.1	2.0	1.5	1.7
E_c *(MPa)*	25300	31800	30200	29200	31700

Legend: $f_{c,cyl}$: compression concrete cylinder strength, determined from 3/4 tests per test unit. f_t: tensile concrete strength, determined from four double-punch tests per test unit according to equation: $f_t = F/\left(\pi\left(1.2rh\text{-}a^2\right)\right)$, where F is the punching force, h and r are the height and the radius of the cylinder respectively, and a is the steel punch radius. E_c: modulus of elasticity determined from the compression tests.

Table 3. Results of rebar tensile tests.

Diameter of the bars	6	16	
Test units	TW1, TW2, TW3, TW4,	TW1	TW4
$f_{s,y}$ *(MPa)*	460	565	515
$f_{s,h}$ *(MPa)*	-[a]	565	515
$f_{s,u}$ *(MPa)*	625	650	618
$\varepsilon_{s,y}$ *(‰)*	2.5	2.7	3.2
$\varepsilon_{s,h}$ *(‰)*	-[a]	27	29
$\varepsilon_{s,u}$ *(‰)*	99	141	127
E_s *(MPa)*	184000	208150	-[b]

Legend: $f_{s,y}$: yield strength. $f_{s,h}$: strength at onset of hardening. $f_{s,u}$: ultimate tensile strength. $\varepsilon_{s,y}$: yield strain. $\varepsilon_{s,h}$: strain at onset of hardening. $\varepsilon_{s,u}$: ultimate tensile strain. E_s: modulus of elasticity.
[a]This steel showed no yield plateau. [b]The value is not provided because of measurement system problems.

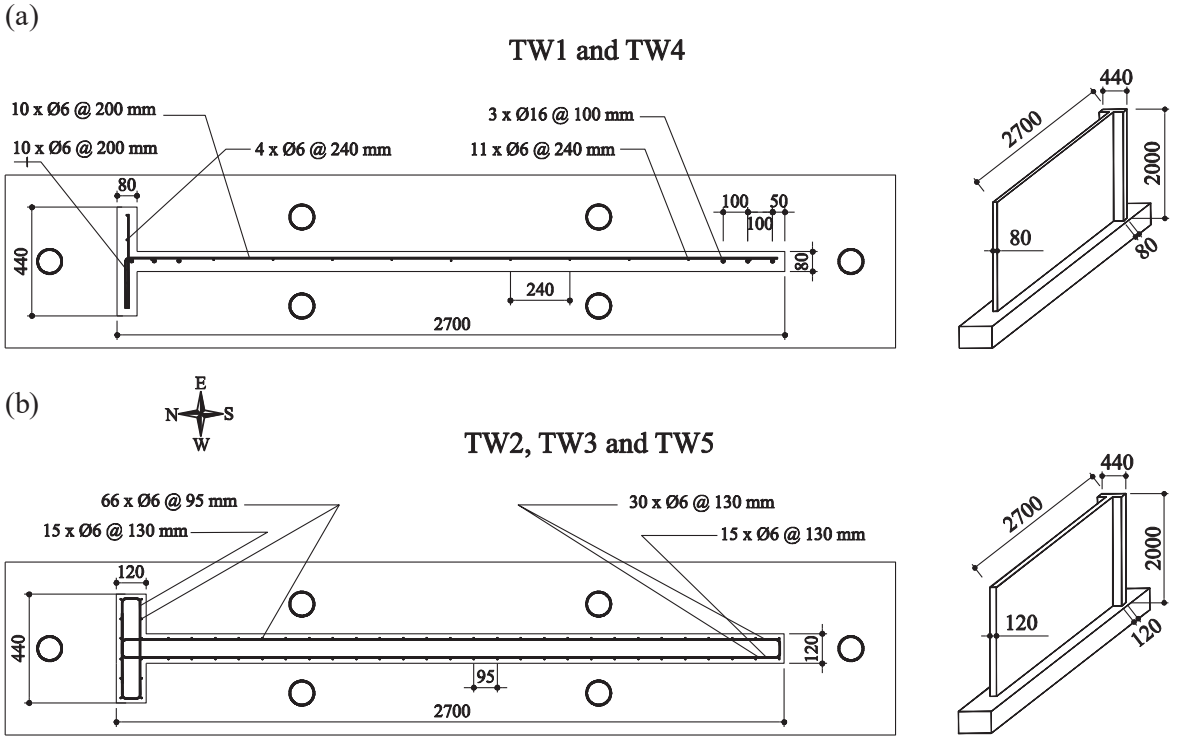

Figure 1. Cross-sectional layout and dimensions of the test units (South-East view, top beam not shown) for walls: (a) TW1, TW4; (b) TW2, TW3, TW5. All dimensions are in mm.

EXPERIMENTAL SETUP AND LOADING PROCEDURE

TEST SETUP

The test setup used for walls TW1, TW2 and TW3 (i.e., subjected to unidirectional loading) is depicted in Figure 2(a), while the modifications put in place for the test of walls TW4 and TW5 are shown in Figure 2(b). The test setup consists of a steel frame, designed to prevent tilting of the wall and to provide a support for the actuators, and a reaction wall. All the steel columns are clamped to the floor with tie rods. Three steel beams are placed over the top RC beam of the test unit to guarantee a distributed application of the loads from the vertical actuators. Such steel loading beams have much larger stiffness and strength than that of the RC wall. Three actuators are employed for the testing of walls TW1, TW2 and TW3: two vertical ones apply the axial load and bending moment corresponding to a chosen shear span ratio through the actuators' lever arm (i.e., the ratio of the moment applied by the vertical actuators to the horizontal force is constant within the test), while the third horizontal actuator applies the cyclic displacement history to the top RC beam of the specimen. The actuators (*Walter+Bai* AG servo-hydraulic actuators with force capacity of ±1000 kN and total stroke of 1000 mm) are controlled in a fully coupled mode such that the axial force and the height of zero moment remained constant throughout the tests. The horizontal actuator is the master while the vertical actuators are slaved to the previous one. Each actuator is equipped with a load cell and a displacement transducer, used to control the deformation rate. Since the hinges of the actuators have some backlash, external linear variable displacement transducers (LVDTs) are used to measure and control the imposed top displacement of each test unit. In the following, the main sides of the specimen will be identified in accordance to the cardinal points of the *EPFL* Laboratory, see Figure 1: North will be referred as the 'flange side' of the wall, while the South extremity will be referred to as 'web edge'. On the East side an optical measurement system is installed, while on the West side digital image correlation measurement systems are used. During the test of walls TW1, TW2 and TW3, the lateral (East-West) stability of the specimen was guaranteed at the storey level through a bracing system consisting of four steel tubes connected to the top RC beam that allowed for free lateral displacements in the in-plane (North-South) loading direction while restricting such movements in the out-of-plane (East-West) direction. The force in these tubes was derived from measurements by strain gages. On the other hand, the possible development of lateral instability modes over the storey height, triggered by in-plane loading, was intentionally not prevented.

(a) (b)

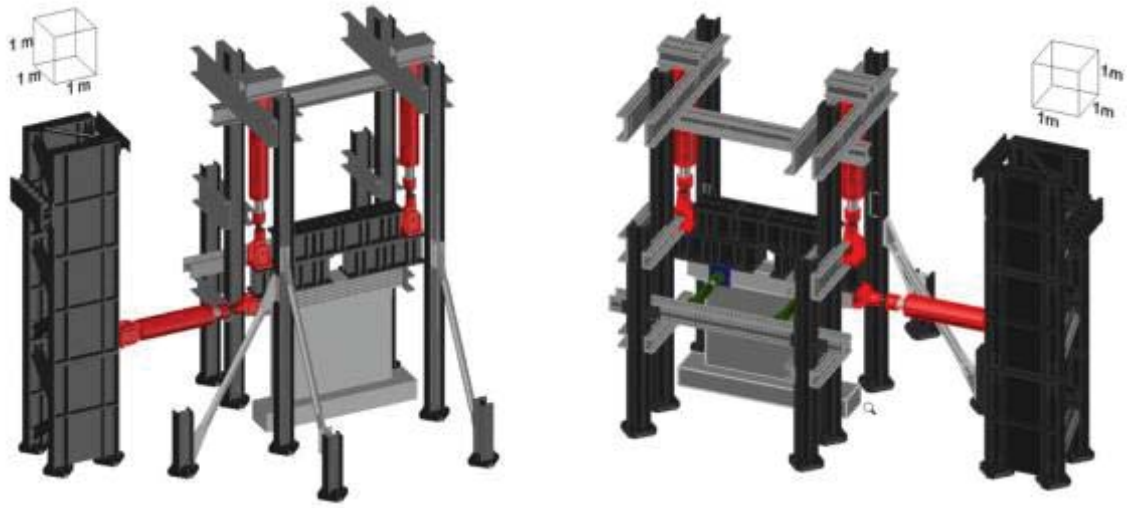

Figure 2. Test setup used for walls: (a) TW1, TW2, TW3 (North-West view); (b) TW4, TW5 (South-East view).

For the tests of walls TW4 and TW5, subjected to bi-directional loading, besides the three actuators previously described, two additional actuators (*Walter+Bai* AG servo-hydraulic actuators with force capacity of ±100 kN and total stroke of 200 mm) are placed to apply the out-of-plane loading. Similarly to the in-plane direction, two external LVDTs are used to measure the out-of-plane top displacement of the test units.

The common approach in RC wall research is to test cantilever walls. Here only a single storey is tested and the top part of the wall is simulated by the two vertical actuators as discussed above. The large steel beam at the top of the RC test unit may influence the shear stiffness and strength of the specimen when compared to a full cantilever wall with multiple storeys (Brueggen 2009). In real structures, a similar though weaker restraint is provided by the storey slabs. Since the objective of this test series was not to test shear critical walls, the approximations introduced by this test setup were judged to be acceptable.

LOADING PROTOCOL

A constant axial load N was applied to the top of the walls such that an axial load ratio of $v = N/f_c' \cdot A_g \cong 5\%$ was attained at the base of the test units (where f'_c is the design mean compressive concrete strength and A_g is the gross wall cross-sectional area). Table 1 shows that, due to the difference between the design mean compressive strength and the results obtained from cylinder tests (performed after the experiments), the applied axial load ratio at the base of the wall actually varied between 3.2% and 4.8%.

The tests were quasi-static cyclic experiments. The loading protocol consisted of a reversed cyclic history applied in deformation control. The peak (positive and negative) values of the imposed (cyclic) drift were named load stages (LS). Figure 3 shows the planned loading protocols for all the test units, while the reader is referred to each of the individual wall test reports for comparison with the actually imposed ones (see section 'Test Data'). Numbering of the load stages started at LS00 (initial measurements) for the unloaded test unit. LS01 corresponded to the application of the axial load. Each target drift (positive and negative) was thereafter numbered successively. The displacements in the out-of-plane direction that were also applied during the tests of TW4 and TW5, in accordance with Figure 3(d) and (e), followed in general the schema depicted in Figure 3(f); for more detailed information the reader is referred to the test report of each wall.

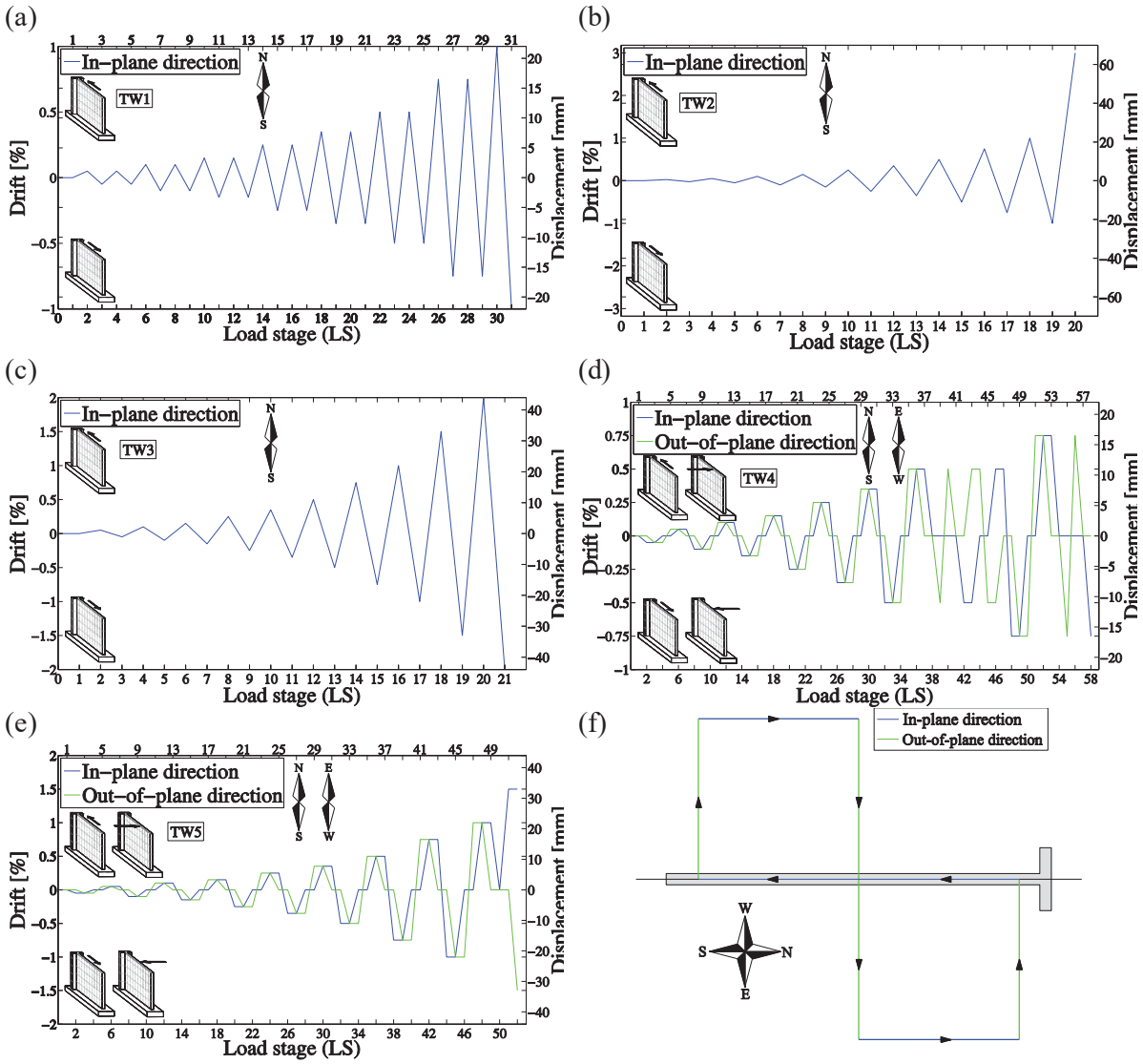

Figure 3. Planned drift history throughout load stages (LS) for walls: (a) TW1; (b) TW2; (c) TW3; (d) TW4; (e) TW5. (f) Typical loading cycle when bi-directional loading was applied.

INSTRUMENTATION

All test units were heavily instrumented using conventional instruments and two optical measurement systems. In addition, crack widths were reported, photos were taken, and videos were recorded.

HARD-WIRED MEASUREMENTS

During the tests up to 54 hard-wired measurements (the actual number depended on the test unit) were recorded. A list of all hard-wired measurements is provided in the test report of each wall.

Vertical LVDTs were placed along the edges of each wall, the configuration of which depended on the test unit. Additional LVDTs were placed on the top RC beam at the actuator height to measure the horizontal displacements. The three-dimensional displacement field along the wall surface was measured through optical measurement systems, as discussed in the next two sub-sections. Additionally, for TW4 and TW5 the rotation of the top beam around the North-South (longitudinal) axis was measured using inclinometers. The horizontal forces were measured by the internal load cells of the actuators.

OPTICAL TRIANGULATION MEASUREMENTS

The three-dimensional displacement field of the surface on the East face of each wall was measured by a grid of infrared light emitting diodes (LEDs). The position of the LEDs was tracked by a camera consisting of three digital optical sensors. To improve the accuracy two cameras were used, each covering about half the wall length. The employed hardware and software was the commercial system NDI Optotrak Certus HD (NDI 2009). The LED grid, whose coordinates were wall-specific, covered the entire wall surface. The LEDs were glued on small metal plates along the grid on the Eastern face of the walls. To measure the displacements of the foundation and of the top RC beam, small L-shaped steel brackets with attached LEDs were glued to these two elements. The LEDs on the top row were hence measuring the displacement of the top beam located 20 mm above, while those on the bottom row measured the displacement of the foundation located 12 mm below.

Upon data post-processing, the LED coordinates were transformed to the following spatial reference system: the x-axis refers to the horizontal in-plane direction of the wall (positive direction from the web to the flange), the y-axis to the vertical in-plane direction (positive direction from bottom to top), while the z-axis refers to the out-of-plane direction (positive

direction from West to East, see Figure 1). The origin of the coordinate system is in the South bottom corner.

The LED data was collected not only during loading (i.e., in-between consecutive load stages), but also during approximately two minutes at each load stage (i.e., for constant values of imposed horizontal displacements).

DIGITAL IMAGE CORRELATION MEASUREMENTS

A speckle pattern for digital image correlation (DIC) measurements was applied on the West face of each wall. As DIC on large surfaces had not been used in the structural engineering laboratory at *EPFL* before, different speckle patterns and camera configurations—sometimes used in parallel—were tested.

For TW1 to TW3, which were subjected to in-plane loading only, a two-dimensional DIC system (DIC system 2D 1) was used. The system was composed of two Nikon D800 cameras, each recording an area of approximately 0.7m x 0.7m at the two bottom wall corners. The exact size and position of these areas varied between walls and is indicated in the test report accompanying each test. For TW3, a second 2D system (DIC system 2D 2) was used. The system was composed of one Canon EOS 5D Mark II camera and recorded the entire wall surface (without the flange). The speckle pattern used for the first three specimens was sprayed with pressured air.

TW4 and TW5 were subjected to bi-directional loading and therefore 3D rather than 2D DIC systems were used. For each wall two 3D systems were used, each recording the entire West face. The first one was composed of two industrial Manta cameras (DIC system 3D 1) and the second one of two Nikon D800 cameras (DIC system 3D 2). The first system recorded black and white photos while all other cameras recorded colour photos. The black and white photos are smaller size files while simultaneously the sensor's larger dimensions mean that they have a higher resolution. The speckle pattern was applied by means of a stencil with a computer generated pattern. The black colour was applied with a spraying can.

CRACK WIDTHS, PHOTOS AND VIDEOS

The maximum crack width, as well as the widths of several cracks developing in the walls, were measured manually at most load stages using a crack-width comparator and are recorded in the lab books, which are made available. Photos of all faces of each test unit were taken at every load stage, as well as of all relevant signs of local damage (cracks, spalling, splitting or

crushing of concrete, rebar buckling and fracture, etc). Moreover, videos of the wall deformation occurring in-between successive load stages were made. These resources proved very useful in the *a posteriori* analysis of the wall behaviour, contributing to a better understanding of the progression of damage and the transfer of forces between distinct deformation modes of the member.

TEST OBSERVATIONS

The following sub-sections present a summary of each member response and a brief discussion on the mechanisms that led to failure.

TW1

Figure 4(a) shows the in-plane force-displacement responses of wall TW1, wherein a stable hysteretic behaviour with appreciable dissipation of energy can be observed. Focusing on the last cycle, i.e. while loading towards -1% drift (LS30→LS31), clear signs of cyclic strength degradation can be observed: upon reaching the target drift of the previous cycle (-0.75%), the in-plane force capacity of the wall was approximately 40% smaller. Continuation of loading led to wall failure due to concrete crushing and buckling of rebars. It is noted that the strength degradation appears to have initiated when returning from positive drifts and approaching zero in-plane drift, where the out-of-plane displacement along the wall height was maximum. At that point, it was apparent that the force-displacement curve deviated from the branch corresponding to the previous loadings towards -0.75% drift.

Cracks following a mainly horizontal pattern started forming from the first loading cycles, indicating a flexural type of behaviour. Although the wall was loaded in-plane, when loading first to -0.75% drift (LS26→LS27), the wall started to show evident out-of-plane displacements along the height towards West, but the latter were recovered completely before reaching the target drift. A similar behaviour with even larger out-of-plane displacements was observed during the second cycle at -0.75% drift (LS28→LS29). During loading at -1% drift, following the large out-of-plane deformations depicted in Figure 4(f) and the progression of concrete crushing, a local buckling of the longitudinal rebars in the bottom region of the web edge took place, see Figure 4(g). The failure mode was thus an in-plane failure triggered by damage induced by out-of-plane deformations (Rosso, Almeida, and Beyer 2016). The splicing of the D6 longitudinal bars did not seem to have affected the wall performance.

TW2

Figure 4(b) shows the force-displacement response of wall TW2. It shows stable hysteretic loops up to -0.75% drift when loading towards the web side (LS17). During the following cycle in the same direction (LS19), at -1% drift, the wall lost almost half of its horizontal force capacity, indicating the attainment of failure. As expected, when loading towards the flange side (even values of load stages), the member depicted a much more ductile response and only showed signs of degrading force capacity above drifts of 1.75%. Failure in this direction can be considered to have occurred at around 2.2% drift, corresponding to an approximate drop of 20% of the member capacity. It should be noted that, in Figure 4(b), there is an abrupt drop in the force-displacement response of the test unit at around 1.2% drift. Such drop does not correspond to any physical phenomenon but rather to the pressing of the 'emergency stop' button of the oil pressure system feeding the actuators. This was done as it was feared that a possible collapse could be imminent, putting at risk the integrity of diverse laboratory equipment (e.g. LVDTs, which were therefore removed).

The first visible crack was detected at LS06, corresponding to a very small drift of 0.1%. Compression crushing of the concrete cover was signalled by the appearance of the first vertical cracks in the web edge of the test unit (LS13). The horizontality of the wall cracks indicates a predominantly flexural type of member behaviour in an initial phase. At load stage LS17, the concrete spalled off along a height of approximately 10 cm at the web edge base.

When continuing loading to LS19, extensive crushing of the concrete at the web edge bottom region took place, which affected the load carrying capacity of the wall and induced the failure of the member in this direction. Hence, it was decided to not reload again the wall in the same direction. During the following load reversal to LS20, the wall showed a stable ductile behaviour up to around 2% drift, at which point concrete cover spalled off.

The progressive loss of the wall capacity beyond 2% drift was not related to concrete crushing in the flange but can be attributed to the consecutive fracture of longitudinal rebars at the (opposite) web edge, which was distinctly heard during the test. Figure 5 shows the condition of the test unit at the end of the experiment. It should be noted that very small out-of-plane displacements were observed (less than 1 cm). Further information about the response of TW2 can be found in Almeida et al. (2015).

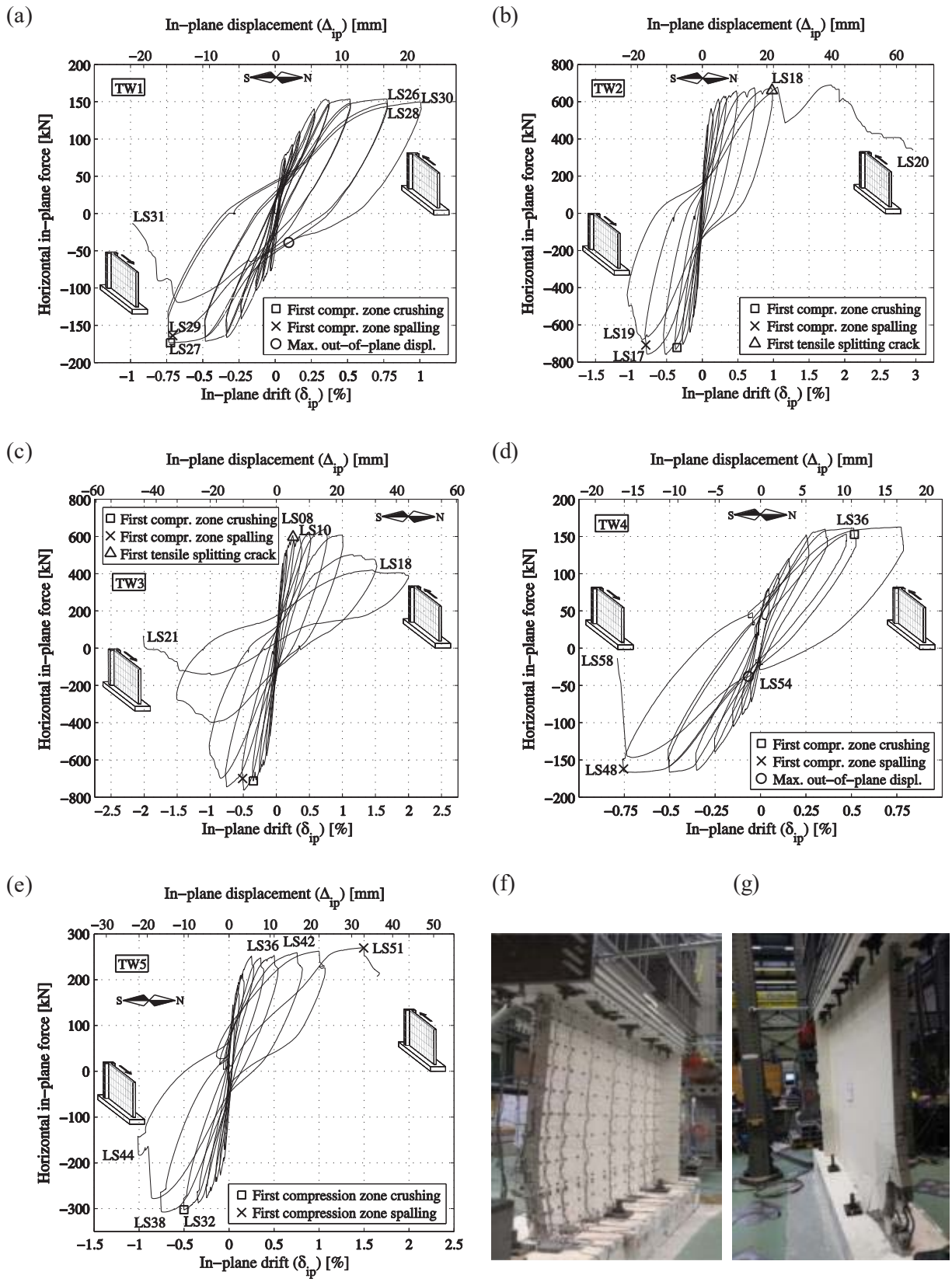

Figure 4. In-plane force-displacement response for walls: (a) TW1; (b) TW2; (c) TW3; (d) TW4; (e) TW5. (f) Deformed shape of wall TW1 when loading to -1% drift. (g) TW1 at the end of the test, after failure.

(a) (b)

Figure 5. (a) Overview of wall TW2 condition at final load stage LS20. (b) Close-ups at web edge, depicting rebar fracture.

TW3

The force-displacement response of wall TW3 is shown in Figure 4(c). Comparing the results of this wall with TW2, it can be observed that the response is quite similar when loading towards the web edge side (negative values of drift). On the other hand, when loading occurs towards the flange edge side (positive values of drift), the test unit does not attain quite the same value of force capacity, and the degradation of strength starts at a lower drift level of 0.75%. The drift level corresponding to an approximate drop of 20% of the member capacity is 1.15%, which represents roughly 50% of the corresponding drift capacity of TW2. The local effects caused by the presence of lap splices can explain this comparative decrease of the wall performance at the global level.

The first face-splitting vertical cracks at the web edge of TW3 appeared as early as load stage LS08 (corresponding to a drift of 0.25%) along the upper half of the lap splices, indicating the significant transfer of tensile stresses between the rebars and the surrounding concrete in the lap splice region, and possibly yielding of the rebar. At LS10 (0.35% drift), a very clear side-splitting crack at the web edge extremity also showed up extending over approximately the entire height of the lap splice.

The crack pattern showed that a concentration of deformation above the lap splice took place. When the web edge was in tension, a single large crack at about the top end of the lap splice opened up (22 cm above the foundation, Figure 6(a)). Simultaneously, the cracks above the lap splice started to reduce their width in comparison with previous load stages. For loading in the other direction, concrete crushing localized in the large crack above the lap splice, see Figure 6(b). An inspection of the aforementioned crack at the end of the test shows that the

tensile failure involved a combination of rebar fracture and bond-slip (Almeida, Prodan, Tarquini, et al. 2016). As already observed for TW2, very small out-of-plane displacements occurred (less than 1 cm).

TW4

Figure 4(d) shows the in-plane force-displacement response of TW4 (it is recalled that both top in-plane and out-of-plane displacements were applied to this wall, as well as for TW5). During the last cycles, when loading from the flange to the web edge, the wall showed clear signs of cyclic strength degradation. During the last loading cycle (towards -0.75% drift), the in-plane capacity of the wall at -0.70% drift was approximately 90% of the strength at the previous cycle at -0.75% drift (LS48), which was then followed by a sudden drop in resistance.

Wall TW4 showed a predominantly flexural behaviour from the first load stages, with the appearance of mainly horizontal cracks. At 0.5% drift (LS36) crushing of the concrete was first observed, occurring at the wall base of the web edge. From LS38 onwards the wall developed an out-of-plane deformed shape towards West (similarly to wall TW1). At -0.75% (LS48) the first concrete spalling took place (Figure 7(a)). During the second cycle at -0.75% drift (LS57→LS58), following progression of concrete crushing and spalling of cover concrete—partially promoted by rebar buckling—a sudden failure took place. After an increase of the overall out-of-plane displacement along the wall height, then completely recovered (Figure 7(b)), the failure involved abrupt concrete crushing and buckling of the rebars in the boundary element of the web edge, as depicted in Figure 7(c). An extensive comparison between TW1 and TW4—which were geometrically identical—can be found in Rosso, Almeida, and Beyer (2016).

TW5

Wall TW5 depicted a relatively fat hysteretic in-plane force-displacement response, as shown in Figure 4(e). This can be associated to the clear predominance of flexural deformations, as evidenced by a stable development of well distributed horizontal cracks along the wall height, both from the flange and the web edges. The vertical distribution of these cracks was much larger than those of the identical wall TW2, as observable from the comparison between Figure 8(a) and Figure 5(a), which is directly attributable to the imposed shear span ratio, almost 2.5 times larger in wall TW5 (see Table 1). Only in the later load

stages, corresponding to larger in-plane drifts, did rather inclined shear cracks show up to bridge between the tensile and compressive zones.

The first horizontal cracks from the web edge appeared at LS06—corresponding to an incipient imposed drift of 0.05% (both in- and out-of-plane), and from the flange edge at LS08—corresponding to an also small in-plane drift of -0.1%. The first vertical crushing cracks were observed at absolute in-plane drifts of 0.5% for both directions (i.e., at LS32 for the web edge, and at LS36 for the flange edge, in the latter case while a simultaneous out-of-plane drift of 0.5% was also being applied). At the following drift level of 0.75%, extensive crushing and concrete spalling occurred while loading towards the web edge (LS38), while in the opposite direction only minimal spall-off could be observed at the flange corner under maximum compression from bi-directional loading (LS42). Finally, specimen failure occurred at LS44 during in-plane loading towards -1% drift: as illustrated in Figure 8(b), generalized crushing at the web edge took place. However, the sudden drop of around 35% on the lateral load capacity can also be ascribed to the buckling of the two outermost layers of longitudinal reinforcement.

When the web edge failed, the flange side was not significantly damaged and therefore the test was continued. After having completed the cycle at 1% drift the wall was unloaded to the zero position and then it was loaded again to the flange direction. After attaining an imposed level of 1.5% in-plane drift (LS51), and while trying to load to -1.5% out-of-plane drift (LS51→LS52), the in-plane force capacity dropped significantly—due to concrete crushing and spalling at the Western side of the flange—and the test was hence stopped.

Apart from this last cycle, the influence of the imposed out-of-plane displacements does not seem to have significantly affected the member response since the load stages corresponding to the application of out-of-plane displacements only minimally influenced the resisting in-plane lateral load, and further produced only a relatively minor increase of pre-existing cracks, concrete crushing and spalling. However, such effect was visible in the flange, suggesting that the study of the effects of out-of-plane loads on barbelled walls may be worth pursuing.

(a) (b)

Figure 6. (a) Load stage LS18 for wall TW3: crack of 35 mm width at about lap splice level (22 cm above the foundation), extending along a length of around 100 cm. (b) Final condition of wall TW3. Crushing from the web edge extends throughout a length of about 220 cm.

(a) (b) (c)

Figure 7. (a) Load stage LS48 for wall TW4: concrete spall-off at the web edge. (b) Final condition of TW4: the relevant out-of-plane displacements that occurred during the test cannot be observed in the final collapsed state. (c) Close-up of rebar buckling after failure.

(a) (b)

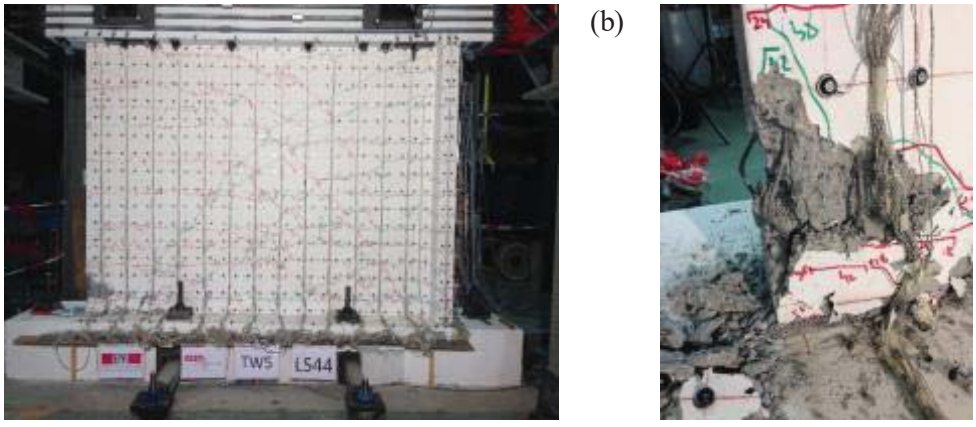

Figure 8. (a) General condition of wall TW5 at horizontal failure (loading towards the web edge, at load stage LS44). (b) Detail of the crushing zone, with buckling of longitudinal rebars.

TEST DATA

ORGANIZATION OF THE DATA

All test data can be downloaded from a publically accessible platform (Almeida, Prodan, Rosso, et al. 2016). The structure of the data folders is summarized in Figure 9. The data is organized by specimen, with specific folders for each test unit "TW(i)", whilst in a further folder ("Overview") copies of the most relevant files are provided. This latter folder is thought for readers who want to get a general idea of the walls' response without downloading the complete data set.

OVERVIEW

The folder "Overview" contains a summary of the five wall tests. Firstly, the test reports for each test unit are provided ("TW(i)_Specimen_description.pdf"). Then, in the sub-folder "Photos", a collection of the most interesting images of the specimens is grouped. The sub-folder "Postprocessed data" contains the post-processed data from the conventional instruments and LEDs for each wall. For a description of these files see the following section.

TW(i) FOLDERS

The data is organized first by specimen. In Figure 9 the folders for a generic wall TW(i) are represented; this data structure corresponds to the most general layout, although for each specimen smaller differences may show up since the instrumentation was not exactly the same for all the tests. Three main folders can be downloaded for each test unit:

1. "TW(i)_General": it contains a test report summarizing the characteristics and the specific test details of wall TW(i) (called "TW(i)_Specimen_description.pdf", which follows the structure of the current paper) and a file with the drawings of the geometry, reinforcement, and instrumentation (called "TW(i)_Construction_and_instrumentation_drawings.dwg"). Additionally, the folder is divided into four sub-levels:

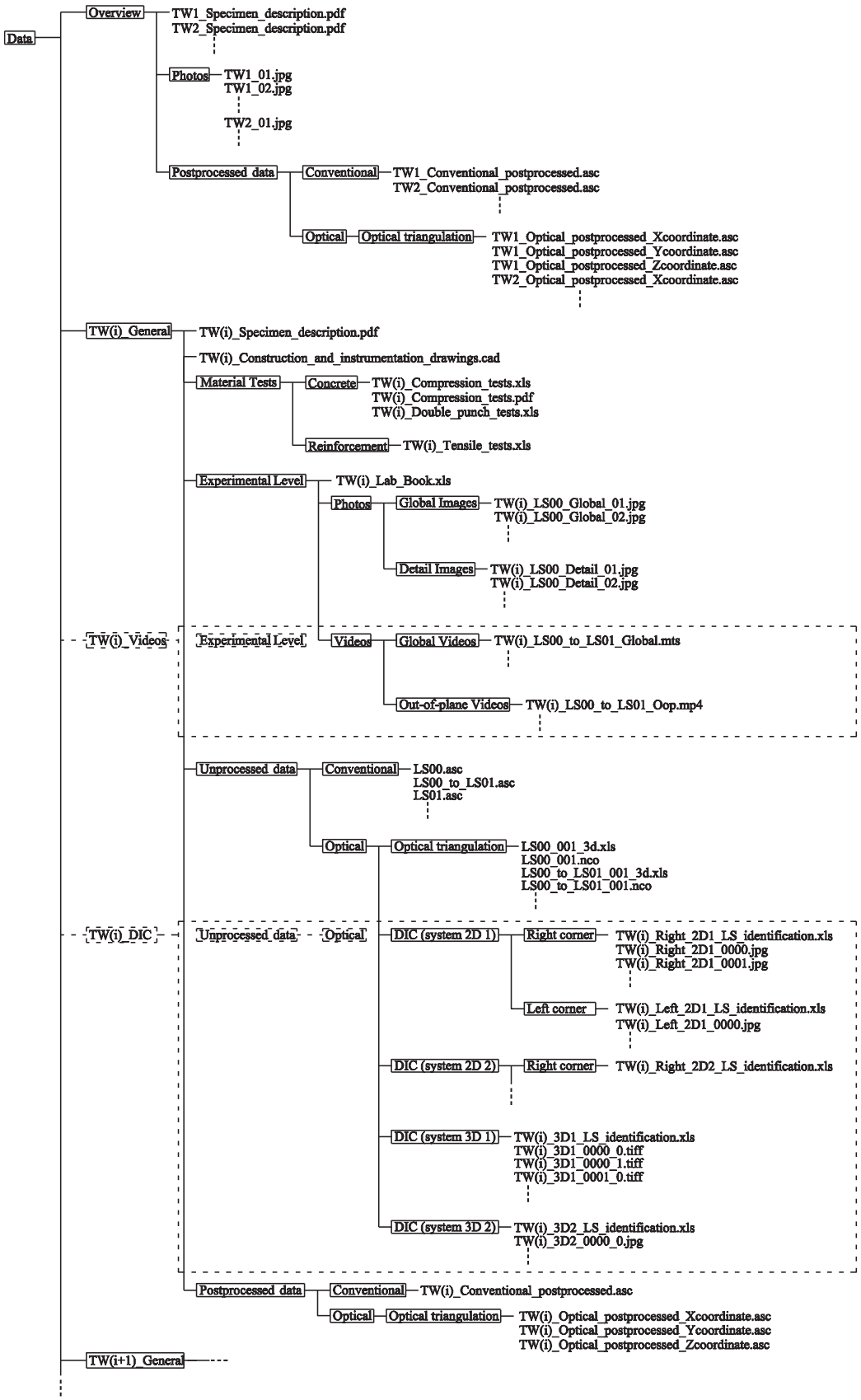

Figure 9. Layout of test data organization (boxes with dotted lines enclose folders that can be downloaded separately from "TW(i)_General").

(i) "Material Tests": two sub-folders contain the results of the material tests performed on the "Concrete" (compression tests and double punch tests) and on the "Reinforcement" (uniaxial tensile tests). Further information on how these tests were carried out can be found in the specific test reports.

(ii) "Experimental Level": a copy of the laboratory notebook, which records observations made during the experimental test, is provided in the form of an Excel spreadsheet (named "TW(i)_Lab_Book.xls"). Two main sub-folders, "Photos" and "Videos", are part of this sub-level. The latter is downloadable in a separate file, see point 2 below ("TW(i)_Videos"). The former collects the main photos of the test; in particular, the sub-folders "Global Images" and "Detail Images" provide images of the entire wall and of interesting details of the specimen (taken at the load stages) respectively. The images and the videos were named "TW(i)_LS(j)" or "TW(i)_LS(j)_to_LS(j+1)" when recorded at a load stage (j) or in-between two load stages (j) and (j+1) respectively.

(iii) "Unprocessed Data": part of the sub-folders forming this sub-level are downloadable in a separate file, see point 3 below ("TW(i)_DIC"). The current file contains the original recordings from the conventional and optical measurement systems; in the "Conventional" folder the original output files of the system *CATMAN* (HBM 2000), used to record the conventional measurements (LVDTs, load cells, …), are collected. It is noted that the channel referring to the optical triangulation system reports simply when the optical system was recording. The conventional measurements were always started before and stopped after the optical measurements and this voltage signal was therefore used to synchronize the two systems. In the folder "Optical triangulation" the outputs from the LED measurement system are collected. For each recording sequence the raw data is provided in an Excel file (extension ".xls") and the sensor settings in NDI-specific file formats (extension ".nco"). In each Excel spreadsheet the actual measurements are organized in columns: the first column stores an index starting from 1, while the following columns give the coordinate measurements of the LEDs (each three columns store the x-, y-, and z-coordinate measurements of one LED respectively). Note that the LED numbers are at this stage still unorganized and the numbering indicated in these files does not correspond to the LED numbering of the processed data. If the LED-coordinates of a LED were not

measured (because the LED was not visible or because it fell off during the test), the columns corresponding to such LED do not contain any entries. The origin of the reference system of the raw data is the centre of the master sensor.

(iv) "Post-processed Data": the optical triangulation data was post-processed in order to synchronize the conventional and the optical measurement systems to reduce the amount of data, and to remove any bias or data that is not linked to the actual behaviour of the test unit (e.g. data was removed when a LED fell off). The data is again divided in two folders: "Conventional" and "Optical". In the file "TW(i)_Conventional_postprocessed.asc", the columns represent a specific measurement—as described in the test report relative to the specimen, "TW(i)_Specimen_description.pdf"—during the entire test; in the files "TW(i)_Optical_postprocessed_(k)coordinate.asc" the first row indicates the LED numbers—according to the description shown in the aforementioned test report—and the corresponding columns below report the measured displacement along the (k) coordinate—x, y or z—of the LED during the test. Note that, due to distinct events that occurred during the experiments—as described in the previous paragraph—some channels were not post-processed up to the last load stage of the test.

2. "TW(i)_Videos": two different video angles were used; from the West the in-plane response of the entire wall was recorded (see folder "Global Videos") while from the South the member response was filmed in order to capture possible out-of-plane displacements (see folder "Out-of-plane Videos"). Due to space constraints, just the last load stages or those considered potentially interesting for the readers were included in the database.

3. "TW(i)_DIC": this folder collects the photos taken for the application of DIC post-processing techniques. Photos from each DIC system are organised in different sub-folders (see section 'Digital Image Correlation Measurements'). In each sub-folder the photos taken during the calibration are the first to be provided, followed by images taken in-between and at the single load stages. In each folder an Excel file (extension ".xls") is provided in which the numbering of the photos is related to the load stages. Note that for the 2D systems, "Right" and "Left" refer to the corresponding corners, while for the 3D systems "_0" refers to the left camera whilst "_1" stands for the right one. Since the cameras of the digital image correlation systems were not connected to the system measuring the conventional instruments, the synchronization between the data and the photos can only be carried out at the level of the

"Unprocessed data" through the corresponding file date settings (all the internal camera clocks were manually synchronized before each test).

EXAMPLES OF DERIVED DATA

This section includes some examples of plots and figures that can be produced using the provided experimental data. All plots are created using the post-processed data.

EXAMPLE PLOTS FOR GLOBAL BEHAVIOUR

The test unit TW1 showed a global behaviour influenced by out-of-plane deformations. The optical measurements taken during the tests allow plotting the evolution of the deformed shapes of the walls. Figure 10(a) depicts the out-of-plane displacement profile of the web edge (i.e., the outermost column of LEDs) in-between several load stages: it can be seen that large values of the out-of-plane displacement were attained.

Test unit TW4 was subjected to bi-directional loading. Figure 10(b) shows the out-of-plane displacement against the in-plane displacement at the height of the horizontal actuators (blue line). It can be compared with the out-of-plane displacement at midheight of the web edge (red line), which shows an asymmetric behaviour for the two in-plane loading directions. When loading towards the web (negative in-plane direction), the out-of-plane displacements at midheight are considerably larger than when the wall is pushed towards the flange (positive in-plane direction). This is because the flange is more stable in compression than the web edge.

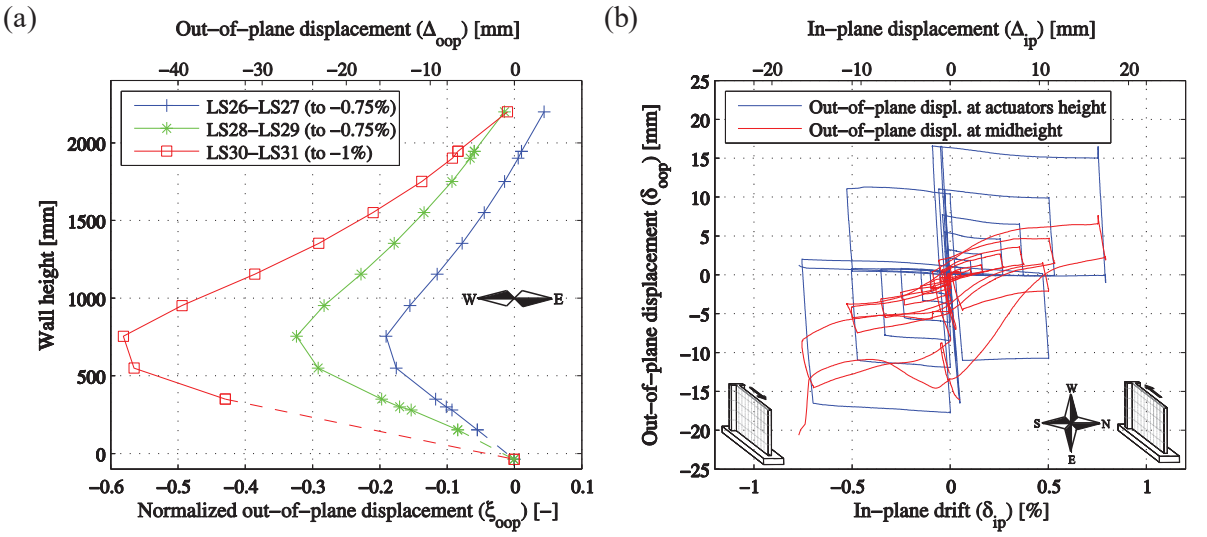

Figure 10. (a) Web edge out-of-plane displacement profile along the wall height between consecutive load stages for wall TW1. (b) In-plane displacement *versus* out-of-plane displacement for wall TW4.

EXAMPLE PLOTS FOR LOCAL BEHAVIOUR

The optical measurement data can also be used to compute local deformations, such as strains and crack widths. Figure 11(a) shows the distribution of the axial vertical strains of TW1 when the maximum out-of-plane displacement along the wall height was attained (i.e., during loading LS30→LS31); the plot points out how the compressive strains concentrate in the web edge at around 755 mm from the base foundation, providing an idea of the band at the wall mid-height in which cracks closure causes the reduction of the global out-of-plane wall deformations.

Test unit TW3 differed from TW2 in the inclusion of lap splices at the wall base. As described in the section 'Test Observations', such constructional detail induced a distinct local and global behaviour of the member. In particular, a large crack formed around the top of the lap splices. In test unit TW2 the deformations spread over a plastic region near the wall base. This difference in behaviour is illustrated in Figure 11(b), which shows, for both test units, the local vertical strains in the web edge region at the crack height; they correspond to the average of the strains from four consecutive pairs of LEDs (along the wall length) above and below the top extremity of the lap splices (i.e., between markers no. 2-3, 18-19, 34-35, and 50-51, see corresponding test reports). It can be seen that, for test unit TW3, strains concentrate at much lower values of in-plane drifts when compared to TW2, putting into evidence the abovementioned differences at the local level.

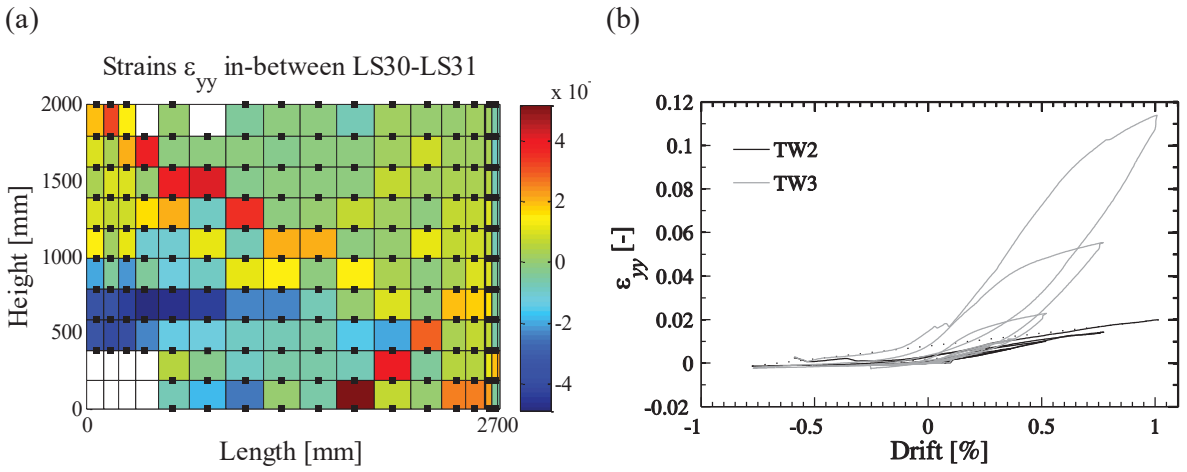

Figure 11. (a) Distribution of local axial vertical strains throughout the wall when the maximum out-of-plane displacement was attained for TW1, during loading LS30→LS31 (the two LED rows at around 340 mm above the base were removed for computation and plotting purposes). (b) Averaged local vertical strains in the web edge region, at a height corresponding to the crack developing at about the top extremity of the lap splices (the last data entries were manually removed for plotting purposes).

SUMMARY

The paper presented the data of five quasi-static cyclic tests on thin T-shaped RC walls, which is made publically accessible. The tests are unique with respect to the following aspects. TW1 and TW4 are the first tests on RC walls that developed large out-of-plane displacements along the wall height for which the entire 3D displacement field was measured. The pair TW1-TW4 allows to compare the response of a wall subjected to uni-directional loading (TW1) to that of an identically constructed specimen subjected to bi-directional loading (TW4). TW3 is the wall test with the largest lap splice length to shear span ratio (among those that the authors could find in the literature) and, when compared to other tests on walls with lap splices, shows therefore the influence of the moment gradient on lap splice performance. The corresponding reference test unit with continuous reinforcement that serves as a benchmark was TW2. Wall TW5 is geometrically and mechanically similar to unit TW2, but was loaded under bi-directional loading (with a larger shear span ratio). Test units TW4 and TW5 are one of the first bi-directional wall tests on nearly rectangular walls and allow therefore to make an initial assessment of the impact of bi-directional loading on wall performance.

The walls tested correspond to the bottom storey of the idealized building, where inelastic deformations concentrate. The axial force, shear force and bending moment that resulted from the upper storeys were simulated by three (in the uni-directional tests) or five (in the bi-directional tests) coupled servo-controlled actuators. The walls were extensively instrumented using conventional instrumentation and two optical measurement systems (an LED-based triangulation system and digital image correlation systems) providing therefore a wealth of information not only at the global but also at the local level. Such data is important to understand wall behaviour but also to validate numerical models.

ACKNOWLEDGMENTS

The testing of test unit TW1 was financed through an *EPFL Seed Money* grant of the *EPFL Cooperation & Development Center (CODEV)*, which was awarded to the *EESD group* (PI) and the *School of Engineering of Antioquia* and the *University of Medellin*, in Colombia (Co-PIs). The reinforcement layout of the wall was designed by the Co-PIs Prof. Carlos Blandon and Prof. Ricardo Bonett. The test units TW2 and TW3 were financed through a grant by the *Stiftung zur Förderung der Denkmalpflege* ("Trust for Cultural Heritage"), which also supported the first author. The second author was supported by a grant of the *University of*

Cluj-Napoca, Romania, as well as a fellowship of the *EPFL,* while the third author was supported by the SNSF grant 200021_132315 "Seismic design and assessment of reinforced concrete core walls - Phase II". All contributions are gratefully acknowledged. The authors would also like to express their sincere appreciation to all engineers, technicians and students who helped with the laboratory testing.

REFERENCES

Almeida, J. P., Prodan, O., Rosso, A., and Beyer, K., 2016. Tests on Thin Reinforced Concrete Walls Subjected to In-Plane and Out-of-Plane Cyclic Loading. figshare. http://doi.org/10.6084/m9.figshare.3490754.v2.

Almeida, J. P., Prodan, O., Tarquini, D., and Beyer, K., 2016. Influence of Lap Splices on the Cyclic Inelastic Response of RC Walls. I: Database Assembly, New Experimental Tests, and Findings for Model Development, *Journal of Structural Engineering* :(Manuscript under review).

Beyer, K., Dazio, A., and Priestley, M. J. N., 2008. Quasi-Static Cyclic Tests of Two U-Shaped Reinforced Concrete Walls, *Journal of Earthquake Engineering* **12**, 1023–53.

Bimschas, M., 2010. *Displacement Based Seismic Assessment of Existing Bridges in Regions of Moderate Seismicity*, *PhD Thesis,* ETH, Zurich, Switzerland.

Birely, A. C., 2012. *Seismic Performance of Slender Reinforced Concrete Structural Walls*, *PhD Thesis,* University of Washington, Washington, U.S.

Brueggen, B. L., 2009. *Performance of T-Shaped Reinforced Concrete Structural Walls under Multi-Directional Loading*, *PhD Thesis,* University of Minnesota, Twin Cities, USA.

Constantin, R., and Beyer, K., 2016. Behaviour of U-Shaped RC Walls under Quasi-Static Cyclic Diagonal Loading, *Engineering Structures* **106**, 36–52.

Elnady, M. E., 2008. *Seismic Rehabilitation of RC Structural Walls*, *PhD Thesis,* McMaster University, Hamilton, Canada.

Elwood, K. J., 2013. Performance of Concrete Buildings in the 22 February 2011 Christchurch Earthquake and Implications for Canadian Codes, *Canadian Journal of Civil Engineering* **40**, 759–76.

Goodsir, W. J., 1985. *The Design of Coupled Frame-Wall Structures for Seismic Actions*, *PhD Thesis,* University of Canterbury, Christchurch, New Zealand.

Hannewald, P., Bimschas, M., and Dazio, A., 2013. *Quasi-Static Cyclic Tests on RC Bridge Piers with Detailing Deficiencies*, *Report Nr. 352 - Institut fur Baustatik und Konstruktion,* ETH, Zurich, Switzerland.

HBM. 2000. Catman Data Acquisition Software.Hottinger Baldwin Messtechnik GmbH,

Darmstadt, Deutschland: http://www.hbm.com/en/menu/products/software/data-acquisition-software.

Johnson, B., 2010. *Anchorage Detailing Effects on Lateral Deformation Components of RC Shear Walls*, *MSc Thesis,* University of Minnesota, Minneapolis, U.S.

Kam, W. Y., Pampanin, S., and Elwood, K., 2011. Seismic Performance of Reinforced Concrete Buildings in the 22 February Christchurch (Lyttleton) Earthquake, *Bulletin of the New Zealand National Society for Earthquake Engineering* **44**, 239–78.

Layssi, H., and Mitchell, D., 2012. Experiments on Seismic Retrofit and Repair of Reinforced Concrete Shear Walls, in *Proceedings of the 6th International Conference on FRP Composites in Civil Engineering (CICE),* Rome, Italy.

NDI, 2009. Optotrak Certus HD, Northern Digital Inc.Waterloo, Ontario, Canada: http://www.ndigital.com/industrial/certushd.php.

Oesterle, R. G., Fiorato, A. E., Johal, L. S., Carpenter, J. E., Russell, H. G., and Corley, W. G., 1976. *Earthquake Resistant Structural Walls - Tests of Isolated Walls*, *Report to National Science Foundation - Portland Cement Association,* Skokie, Illinois, U.S.

Paterson, J., and Mitchell, D., 2003. Seismic Retrofit of Shear Walls with Headed Bars and Carbon Fiber Wrap, *Journal of Structural Engineering* **129**, 606–14.

Reynouard, J. M., and Fardis, M. N., 1993. *Shear Wall Structures*, *ECOEST/ICONS Thematic report. No 5 - LNEC-National Laboratory of Civil Engineering,* Lisbon, Portugal.

Rosso, A., Almeida, J. P., and Beyer, K., 2016. Stability of Thin Reinforced Concrete Walls under Cyclic Loads: State-of-the-Art and New Experimental Findings, *Bulletin of Earthquake Engineering* **14**, 455–84.

Sritharan, S., Beyer, K., Henry, R. S., Chai, Y. H., Kowalsky, M. and Bull, D., 2014. Understanding Poor Seismic Performance of Concrete Walls and Design Implications, *Earthquake Spectra* **30**, 307–34.

Thomsen, J. H., and Wallace, J. W., 1995. *Displacement Based Design of Reinforced Concrete Structural Walls: An Experimental Investigation of Walls with Rectangular and T-Shaped Cross-Sections*, *Report No. CU/CEE-95-06 - Departement of Civil and Environmental Engineering,* Clarkson University, Postdam, U.S.

Villalobos, E. J., 2014. *Seismic Response of Structural Walls with Geometric Reinforcement Discontinuities*, *PhD Thesis,* Purdue University, Indiana, U.S.

Wallace, J. W., Massone, L. M., Bonelli, P., Dragovich, J., Lagos, R., Lüders, C., and Moehle, J., 2012. Damage and Implications for Seismic Design of RC Structural Wall Buildings. *Earthquake Spectra* **28**, S281–99.